Desalination and Water Treatment
www.deswater.com

doi: 10.5004/dwt.2020.26165

202 (2020) 450–461
October

Synthesis, characterization, and evaluations of Cu-doped TiO_2/Bi_2O_3 nanocomposite for Direct red 16 azo dye decolorization under visible light irradiation

Vahid Barahimi[a,*], Arjomand Mehrabani-Zeinabad[a], Mohammad Rahmati[a], Masoud Ghafaripoor[b]

[a]*Department of Chemical Engineering, Isfahan University of Technology, Iran, Tel. +8415683111; emails: vahid.barahimi13@gmail.com (V. Barahimi), arjomand@iut.ac.ir (A. Mehrabani-Zeinabad), m.rahmati371@gmail.com (M. Rahmati)*
[b]*Department of Materials Engineering, Isfahan University of Technology, Iran, Tel. +8415683111; email: masoud.ghafaripoor@gmail.com (M. Ghafaripoor)*

Received 1 December 2019; Accepted 21 May 2020

ABSTRACT

In this study, a statistical analysis based on the response surface methodology (RSM) was employed to investigate the individual and interaction effects of critical operating and dopant concentration on photocatalytic decolorization of Direct Red 16 under visible-light by Cu-doped TiO_2/Bi_2O_3. Cu-doped TiO_2/Bi_2O_3 is a visible-light-driven nano-catalyst which was synthesized by applying the sol–gel technology for the removal of Direct Red 16. The studied operating parameters include the Bi_2O_3/TiO_2 ratio, Cu/Ti ratio, and reaction time. The statistics-based experimental design and RSM were utilized to find a quadratic model as a functional relationship between the decolorization efficiency and the three operating parameters. Initially, the optimum ranges of Cu/Ti and Bi_2O_3/TiO_2 compounds on the removal of the dye pollution were experimentally obtained, which is 2, 4, and 6 wt.% for Cu/Ti ratio and 8, 9, and 10 wt.% for the Bi_2O_3/TiO_2 ratio. Then, a set of TiO_2/Bi_2O_3-Cu nano-catalysts with various ingredients was synthesized based on the RSM method, and field emission scanning electron microscopy, diffuse reflection spectroscopy, and X-ray diffraction were performed. The performed experiments on the removal of the pollution showed that the produced nano-catalyst with 6 wt.% Cu/Ti ratio, 8 wt.% Bi_2O_3/TiO_2 ratio and reaction time of 3 h had the maximum removal efficiency of 99%. The regression analysis with an R^2 value of 0.99 showed the right consistency between the model prediction and experimental data of the decolorization efficiency. Using the quadratic model of RSM, the optimum contents of the nano-catalyst was 5.9 wt.% Cu/Ti ratio and 8.0 wt.% Bi_2O_3/TiO_2 ratio with a removal efficiency of 99.4% while the efficiency of the experiments was 99.0% ± 0.7% by application of this synthesized nano-catalyst.

Keywords: Azo dye decolorization; TiO_2/Bi_2O_3-Cu nano-catalysts; RSM; Visible light

1. Introduction

Today, the presence of dyes and organic pollutants of industries in our natural water and wastewater constitutes a significant problem [1]. Textile wastewater containing dyes, detergents, acids, organic compounds, and heavy metals is a global environmental problem [2–4]. Due to their intense color, the paints represent a major ecological problem, and their treatment is a necessary step before discharging them into the aquatic environment, and physical and chemical methods are currently being used to eliminate them. However, such methods do not destroy the pollutants

* Corresponding author.

but only transfer them from the liquid to the solid phase, and their reconstruction requires investment [5]. Azo dyes, known as p-bond nitrogen, are the most widely used synthetic dyes and are generally critical industrial wastewaters. Due to their slow degradation and toxicity, these dyes are classified as hazardous substances [6]. One of the dyes used in the textile industry is Direct red 16. This dye is azo and therefore pollutes the environment [7,8].

Photocatalytic and advanced oxidation processes (AOPs) play an essential role in the drinking water and wastewater treatment industry. Photocatalytic processes break down the organic compounds into non-toxic minerals [3,9]. Soluble organic dyes are an extraordinary group of industrial wastewater pollutants that must be removed before discharging the treated wastewater to the environment or its reuse [10]. Various semiconductors such as TiO_2, Fe_2O_3, ZnO, CdS, and WO_3 had been used in photocatalytic processes [11]. As a consequence of TiO_2 properties such as high photocatalytic value, non-toxicity, sustainability, and reasonable price, it becomes the most popular photocatalyst. TiO_2 is the most popular photocatalyst because of its unique properties such as high photocatalytic value, non-toxicity, sustainability, and reasonable price [9,12,13]. There are many research studies on the application of TiO_2 under ultraviolet (UV) radiations in photocatalytic processes for the decolorization of azo dyes [14].

In a photocatalytic process, radiation of the light to the nano-catalyst results in the excitation of electrons and the formation of holes [15]. The photocatalytic process depends on conducting a photochemical reaction on the semiconductor surface, which has two primary reactions. The first one includes oxidation from the positive hole, and the second one is a reduction from the negative electron [16].

The goal of researchers is the improvement of efficiency and selectivity of nano-catalyst TiO_2 for various applications. TiO_2 is among the most widely-used materials for the photodegradation process [16], but the performance of TiO_2 for the visible application is greatly restricted because of its wide band gap, which brings some drawbacks [17]. TiO_2 has a wide band gap that is activated by ultraviolet radiation with $\lambda < 400$ nm [18,19]. Doping of TiO_2 with a metal/non-metal element reduces the TiO_2 band gap [20]. Metals such as Cr, Mn, Fe, Ag, V, and Cu and non-metals such as C, N, S, Si, and F can be used for doping [21–23].

Also, the low quantum yield rate of visible light activation is another major drawback [17]. To overcome this shortcoming, TiO_2 can be coupled with narrow band gap semiconductors such as Bi_2WO_4, WO_3, ZnO, $FeTiO_3$, SiO_2, CdS, Bi_2O_3, and Al_2O_3 [24]. Bi_2O_3 with a band gap of 2.8 is widely applied as a visible driven photocatalyst. However, it has low quantum efficiency [17,25]. The TiO_2/Bi_2O_3 heterojunction not only decreases the band gap of TiO_2 into the visible region but also faciles the separation of charge carriers during the photodegradation process [17,25,26].

In this work, the focus is given on modified TiO_2, and a set of nano-catalysts was synthesized by doping of Cu and coupling Bi_2O_3 with TiO_2 with various loadings that were optimized based on the RSM. The synthesized nano-catalysts were used to decolorize Direct Red 16 dye. Direct Red 16 decolorization was also modeled and optimized using the central composite design (CCD).

2. Experimental and methods

2.1. Material

Titanium tetraisopropoxide (TTIP) and isopropanol were used for the synthesis of the catalysts in the current study. To modify TiO_2, $Bi(NO_3)_3{\cdot}5H_2O$, and $CuN_2O_6{\cdot}3H_2O$ were used as the precursors of Cu and Bi, respectively. During the preparation of the TiO_2/Bi_2O_3-Cu solution, the solution pH was adjusted by the addition of HCl and NaOH. A list of materials used in the experimental study is presented in Table 1.

2.2. Synthesis of TiO_2/Bi_2O_3-Cu by the sol–gel technology

In order to control the process of synthesizing nanocrystalline TiO_2 powder, hydrolysis of TTIP in the mixture of isopropanol and deionized water was used. Achieve to reduced rate of the hydrolysis process results in the synthesis of TiO_2 powders revealing favorable optical transparency, porosity, and thermal stability [27,28].

Grześkowiak et al. [28] reported that titania synthesized via hydrolysis of titanium (IV) isopropoxide (TTIP) and calcined at 400°C in air for a period of 3 h. It was consists of just anatase phase and the material did not contain carbon originating from the solvent or from the additives used to stimulate pH. TiO_2 thin films with different titanium isopropoxide (TTIP): acetylacetone (AcacH) molar ratios in solution were prepared by the chemical spray pyrolysis method [29]. Titania (TiO_2) photocatalysts are produced using the hydrolysis of TTIP at 100°C–600°C [30].

The first solution was prepared by dissolving 0.024 g of copper nitrate nanohydrate in 5 mL isopropanol, and the mixture was stirred for 1 h. The second solution was resulted from solving 0.098 g of bismuth nitrate nanohydrate

Table 1
List of used chemicals

Materials	Chemical formula	Purity (wt.%)	Manufactured company
Titanium tetraisopropoxide (TTIP)	$C_{12}H_{28}O_4Ti$	99.999	Merck KgaA, Darmstadt, Germany
Isopropanol	C_3H_7OH	99.5	Sigma–Aldrich
Copper nitrate nanohydrate	$Cu(NO_3)_2{\cdot}3H_2O$	99.99	Merck KgaA, Darmstadt, Germany
Bismuth nitrate nanohydrate	$Bi(NO_3)_3{\cdot}5H_2O$	99.99	Merck KgaA, Darmstadt, Germany
Hydrochloric acid	HCl	37	Merck KgaA, Darmstadt, Germany
Direct Red 16	$C_{26}H_{17}N_5Na_2O_8S_2$	100	Ningbo

in 10 mL isopropanol, and the mixture was stirred for 12 h. For adjusting the pH between 2 and 3, three drops of HCl were added to the solution [31]. The third solution, for the synthesis of Cu-doped TiO_2 nano-catalyst, solution number of 1 was mixed with 3 mL TTIP and 35 mL isopropanol (Fig. 1a). The solution pH was kept within the range of 2–3 by HCl. The prepared solution was ultrasonicated for 20 min and stirred continuously for 12 h. For the synthesis of TiO_2/Bi_2O_3-Cu nano-catalyst, the second solution was added to the third solution, and the prepared solution was ultrasonicated for 20 min and stirred continuously for 12 h (Fig. 1b). The nano-catalysts were placed in an oven at 60°C for 12 h and then were calcined by leaving it in a furnace at 500°C for 2 h.

2.3. Photoreactor

The photocatalytic experiments were conducted in a batch glass cylindrical reactor with an inner diameter of 70 mm, the height of 100 mm, and liquid hold up to 100 mL. The reactor was equipped with an LED light source 12V/30 W and a magnetic stirrer for homogenizing the mixture during the experiment.

2.4. Nano-catalyst characterization

The X-ray diffraction (XRD) pattern of the synthesized nano-catalyst was recorded by a Philips (X'pert Pro MPD, Almelo, Netherlands) X-ray diffractometer with Ni-filtered Cu K_α radiation (wavelength 1.5406 Å) equipped with a Ni filter. Diffuse reflection spectroscopy UV-Vis (DRS) was used to determine the band gap energy of the nano-catalyst and to investigate the effect of type and amount of Cu and Bi_2O_3 on the diffuse reflection spectroscopy UV-Vis.

Also, the morphology of the surface structure of the synthesized nanoparticles was investigated by a field emission scanning electron microscopy (TESCAN FE-SEM MIRA3, Kohoutovice, Czech Republic).

2.5. Procedure and analysis

The decolorization of Direct Red 16 from aqueous solution was investigated under the irradiation of visible light. In order to measure the photocatalytic activity, experiments were done in a batch reactor containing the 100 mL dye solution with a concentration of 25 mg/L. After the addition of 1 g/L of the nano-catalyst, the solution was stirred at a mixing rate of 600 rpm. Initially, the solution was stirred in the dark for 30 min to have a complete equilibrium between solution and nano-catalyst. Then, the solution was mixed for 3 h under the radiation of visible light. All of the experiments were performed at a pH of 6.8. For analyzing tests, 5 mL of the solution samples were centrifuged with a speed of 5,000 rpm for 15 min to separate the nano-catalyst particles. A UV-Vis spectrophotometer at a wavelength of 526 nm was used for measuring the dye concentration. The photocatalytic decolorization efficiency was calculated according to Eq. (1).

$$\text{Removal}(\%) = \left(1 - \frac{C_t}{C_0}\right) \times 100 \quad (1)$$

where C_0 and C_t are the initial and the final concentrations of dye in the solution, respectively.

2.6. Experimental design and statistical analysis

RSM was employed to evaluate the effect of two-component loadings (Bi_2O_3/TiO_2 ratio (*A*, wt.%), Cu/Ti ratio (*B*, wt.%)) and operational parameters (time (*C*, min)) on the Direct Red 16 decolorization under visible light illumination. The three parameters (*A*, *B*, *C*) were chosen as independent variables, while the decolorization efficiency of Direct red 16 was the output response. The experimental ranges and the levels of the independent variables for Direct red 16 photocatalytic decolorization are shown in Table 2. The preliminary screening experiments were used to obtain effective

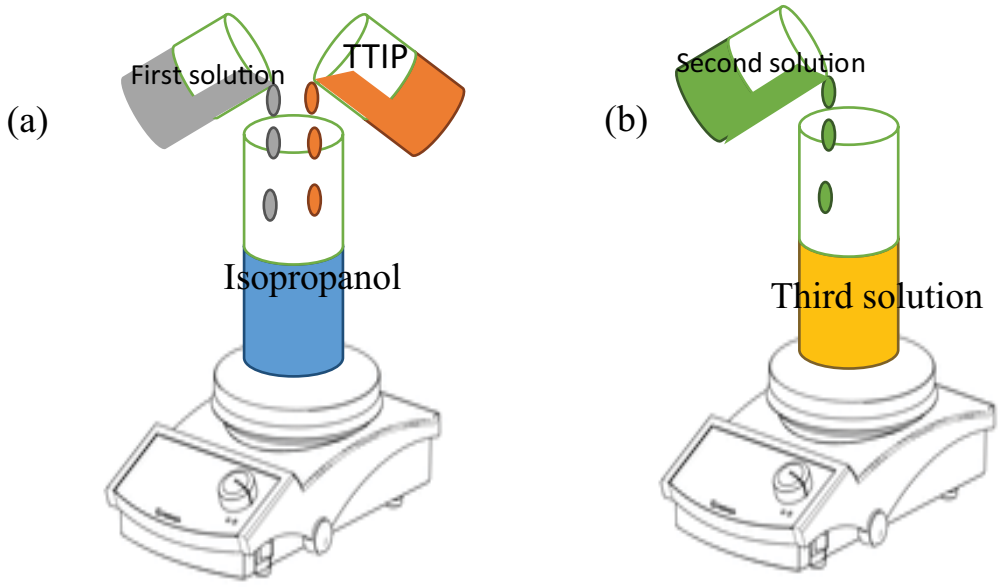

Fig. 1. Synthesis nanocatalyst (a) Cu-TiO_2 and (b) TiO_2/Bi_2O_3-Cu.

Bi_2O_3/TiO_2 and Cu/Ti concentrations values. Based on the results of these experiments that are presented in Fig. 2, the best-produced nano-catalyst for removal of the dye contained 9 wt.% Bi_2O_3/TiO_2 and 4 wt.% Cu/Ti. According to the preliminary experiments, the values of 2, 4, and 6 wt.% for Cu/Ti ratio and the values of 8, 9, and 10 wt.% for the Bi_2O_3/TiO_2 ratio were selected for further experiments. The RSM based on the central composite experimental design (CCD), which is one of the most usual methods of using a response surface methodological approach, was utilized to evaluate the combined effects of the three independent variables using twenty experiment data [25].

Moreover, a quadratic equation was obtained to relate the response variable to the three independent variables, as follows:

$$Y = a_{00} + a_{01}A + a_{02}B + a_{03}C + a_{12}AB + a_{13}AC + a_{23}BC + a_{11}A^2 + a_{22}B^2 + a_{33}C^2 \quad (2)$$

Where Y (%) is the predicted response (decolorization efficiency of Direct red 16), a_{ij} are the coefficients and A, B, and C are the values of independent variables (Bi_2O_3/TiO_2 ratio, Cu/Ti ratio, and time, respectively). Decolorization conditions determined by the CCD method along with the predicted and experimental values of the response are presented in Table 3. Data were analyzed by the analysis of variance (ANOVA), and the optimal values of the variables were obtained using the Design Expert software.

Table 2
Ranges and values of the variables for experimental design

Ranges and values	Variables	–1	0	+1
Bi_2O_3/TiO_2 ratio (wt.%)	A	8	9	10
Cu/Ti ratio (wt.%)	B	2	4	6
Time (h)	C	1	2	3

3. Results and discussion

3.1. X-ray diffraction

XRD patterns of the modified TiO_2 is shown in Fig. 3. The characteristic peaks can be well indexed to the anatase phase anatase TiO_2. The sharp and symmetrical diffraction peaks of pure synthesized TiO_2 show the high crystallinity of the studied sample. Based on the pattern of this figure, no diffraction peaks of Cu^{2+} are detected, which can be due to the low doping amount or excellent size of Cu^{2+} cation (radius of Cu^{2+} = 73 pm and Ti^{3+} = 88 pm [26]). Furthermore, as a result of the lack of Cu separation, clustering, or oxide formation complete dissolution of Cu^{2+} cations for the formation of Cu–O–Ti bonds occurred [18]. Besides, no visible diffraction peaks of Bi_2O_3 was observed in the XRD patterns for TiO_2/Bi_2O_3-Cu. That implies a perfect dispersion of the Bi_2O_3 particles. This issue has been reported by Kumar and Devi [19].

The average crystalline sizes can be calculated based on the anatase diffraction peaks using the Debye–Scherrer equation [32]:

$$D = \frac{k\lambda}{\beta\cos\theta} \quad (3)$$

where D is the crystalline size, λ stands for the wavelength of X-ray (nm), and k is considered to be 0.89, assuming that the particles are spherical. β is the full width in radius at half maximum (FWHM) of the highest peak (rad), and θ represents the Bragg angle of the highest peak. The results given in Table 4 show that a reduction in the crystallite size leads to

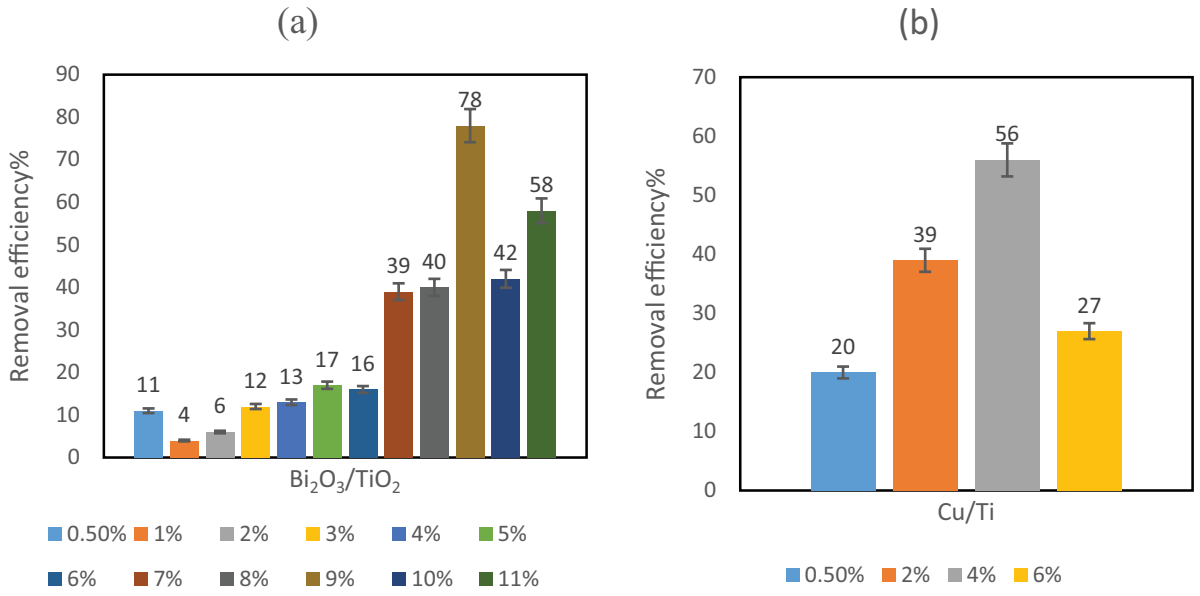

Fig. 2. Removal efficiency of the photocatalytic decolorization reaction: (a) pH = 6.8, [Bi_2O_3/TiO_2] = 1 g/L, C_0 = 25 mg/L reaction time = 3 h and (b) pH = 6.8, [TiO_2-Cu] = 1 g/L, C_0 = 25 mg/L, and reaction time = 3 h.

Table 3
Experimental design matrix and the value of responses based on the experiment runs

Run	Bi_2O_3/TiO_2 ratio (wt.%)	Cu/Ti ratio (wt.%)	Time (h)	Actual decolorization efficiency (%)	Predicted decolorization efficiency (%)
1	9	4	2	65	65.6
2	10	4	2	67	66.2
3	9	4	1	44	44.3
4	8	6	3	99	99.5
5	8	6	1	56	55.6
6	9	4	2	64	65.6
7	9	4	2	66	65.6
8	10	2	3	97	97.7
9	10	6	3	59	59.6
10	8	4	2	64	64.9
11	10	6	1	21	21.2
12	9	4	3	88	85.8
13	9	2	2	53	52.6
14	9	6	2	59	57.1
15	8	2	1	23	22.9
16	8	2	3	45	45
17	9	4	2	67	65.6
18	9	4	2	64	65.6
19	10	2	1	51	50.9
20	9	4	2	66	65.6

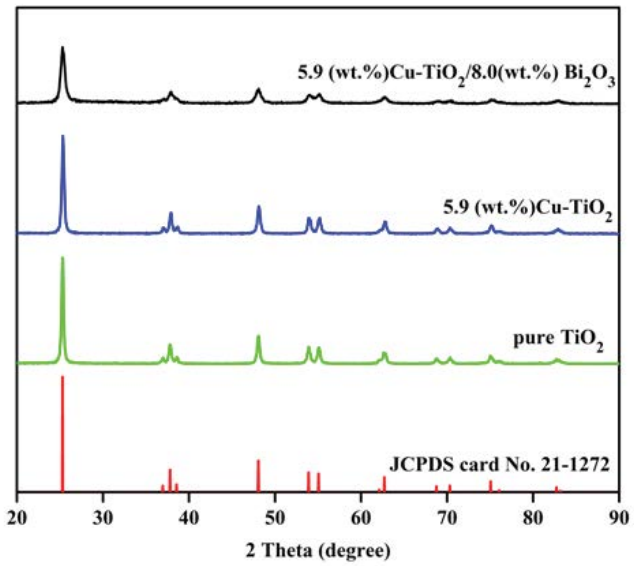

Fig. 3. XRD patterns of the modified TiO_2.

distortion in the lattice structure of the modified TiO_2 due to the modifying process.

3.2. UV-vis DRS

The band gap of the TiO_2 synthesized nanocatalyst was determined using the UV-Vis spectrum. The obtained absorption spectra are shown in Fig. 4. The pure TiO_2 absorption spectrum includes an absorption peak of about 360 nm, due to the transfer of electrons from the valence band to the conduction band. In the DRS spectrum of the nano-catalyst 5.9 (wt.%) Cu-TiO_2, the absorption peak was observed in the region of 420 nm, which is the result of the introduction of copper metals in the structure of TiO_2. This issue results in transferring of absorption from UV spectra to the visible one.

The band gap energy of the nanocatalyst 5.9 (wt.%) Cu-TiO_2/8.0 (wt.%) Bi_2O_3 was also represented in Fig. 4, which shows a broad absorption peak in the 460 nm region. By modifying TiO_2 with Bi_2O_3 semiconductor, its absorption was increased from 420 to 460 nm, indicating a decrease in the band gap energy of the synthesized nanocatalyst. The bang gap energy values are also shown in Table 5.

Table 4
Crystalline size for the modified TiO_2

Samples	Crystalline size (nm)
Pure synthesized TiO_2	32.1
5.9 (wt.%) Cu-TiO_2	26.8
5.9 (wt.%) Cu-TiO_2/8.0 (wt.%) Bi_2O_3	17.7

3.3. Field emission scanning electron microscopy

The morphology of samples pure TiO_2, 5.9 (wt.%) Cu-TiO_2 and 5.9 (wt.%) Cu-TiO_2/8.0(wt.%) Bi_2O_3 is shown

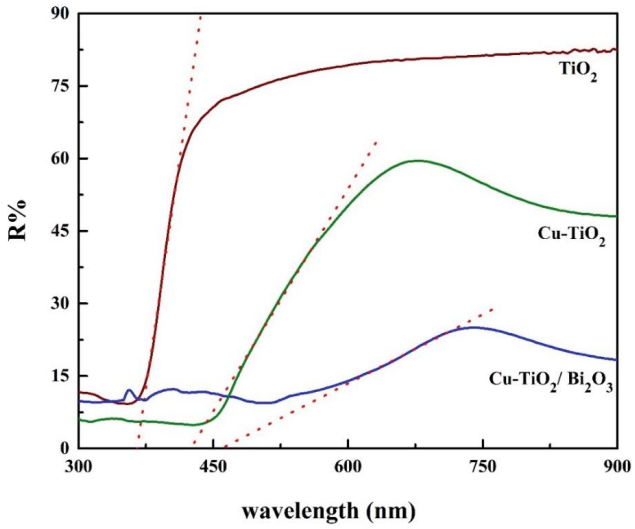

Fig. 4. DRS patterns of the modified nano-catalyst TiO_2.

Table 5
Band gap energy of the modified nano-catalyst

Samples	Band gap energy (eV)
Pure synthesized TiO_2	3.4
5.9 (wt.%) Cu-TiO_2	2.9
5.9 (wt.%) Cu-TiO_2/8.0 (wt.%) Bi_2O_3	2.7

in Fig. 5. Reduction in the size of the particles results in higher uniformity, and the spherical structure of a modifying nanocatalyst. The particle size measured in the field emission scanning electron microscopy (FE-SEM) test is shown. The process of reducing the particle size remains the process of reducing particle size using the XRD test. As shown in Fig. 5, by modifying the nanocatalyst, the particle size was reduced, which increases the contact area.

3.4. Model fitting and statistical analysis

The gained experimental data were analyzed, and a quadratic model is proposed. ANOVA investigated variables impact, their interaction in experiments, and studying the significance of the model. ANOVA investigated the effect of variables and their interaction in experiments as well as studying the significance of the model. In this case, the quadratic model is selected, and its ANOVA analysis is shown in Table 6. The model *p* and *F*-values were used as a tool to check the relative significance of the variables. In general, coefficients with higher *F*-value and lower *p*-value indicate that their corresponding variables have more significance in comparison to other variables [33]. In this case, *p*-value higher than 0.05 shows that the parameter is ineffective on the model, and according to Table 6, the most significant *p*-value belongs to parameter A^2 and eliminating this parameter leads to a more appropriate model. As can be seen in Table 7, all *p*-value parameters are below 0.05, which indicates the effect of these parameters in the model, and using these parameters, a suitable model for data analysis is obtained. Besides the very low model *p*-value, the model *F*-value of 880.27 also showed the adequacy of the model since it was much higher than the theoretical *F*-value. Also, a lack of fit *F*-value of 0.83 indicated good predictability of the model, which implied that lack of fit was not significant relative to the pure error.

Based on the Direct red 16 photocatalytic decolorization results, the following quadratic model was obtained:

$$(\text{Efficiency }\%)^{0.43} = -11.55724 + 1.53791 \times A + 4.78710 \times B + 0.018588 \times C - 0.43535 \times AB + 0.11776 \times AC + 0.038939 \times BC - 0.11217 \times B^2 - 0.098027 \times C^2 \quad (4)$$

The positive coefficients (*A*, *B*, *C*, *AC*, and *BC*) resulted in an increase in the decolorization efficiency, while negative coefficients (*AB*, B^2, and C^2) affected the decolorization efficiency. The model adequacy was further checked using the diagnostic plots (Figs. 6 and 7). As can be seen in figures, the values of R^2 and Adj. R^2 were calculated as 0.998 and 0.997, respectively, implying that the experimental data were fitted very well by the proposed model. In addition to the correlation coefficient, the normal probability plot of the externally studentized residuals was also studied to evaluate the adequacy of the model Fig. 6. According to Fig. 6, the extra points fell near to the straight line, indicating that there was almost no severe departure of the assumptions underlying the analysis and also a good agreement between the actual and predicted values.

The plot of the externally studentized residuals vs. predicted responses is illustrated in Fig. 7. As shown in this figure, all design points of the experimental runs were randomly scattered within the constant range of residuals across the graph (±4.00453), suggesting that the variance of the original observations is constant for all values of the response and the approximation of the fitted model to the response surface was quite acceptable and adequate [34].

3.5. Analysis of response surface

The effects of the operating and nano-catalyst parameters and their interaction effect on the decolorization efficiency of Direct Red 16 are graphically represented by three-dimensional RSM plots and two-dimensional contour plots in Fig. 8.

As shown in Fig. 8a, at low values of Bi_2O_3/TiO_2 ratio, efficiency is low unless Cu/Ti ratio values are high. In fact, at low values of Bi_2O_3/TiO_2 and Cu/Ti ratios, the nano-catalyst band gap energy is high, and the used light source cannot activate the nano-catalyst that results in low efficiency of the nano-catalyst. Furthermore, at lower values of Cu/Ti ratio, higher values of Bi_2O_3/TiO_2 ratio result in a reduction of the nano-catalyst bandgap energy. This issue is due to the occurrence of the recombination phenomenon in the nano-catalyst by increasing doping values to an optimum level [35]. On the other hand, for higher values of both Bi_2O_3/TiO_2 and Cu/Ti ratios, the efficiency decreases. As shown in Fig. 8b, increasing as expected by processing time, the decolorization efficiency is enhanced. The photocatalytic process is a time-consuming process. In the current study, modified nano-catalyst will examine

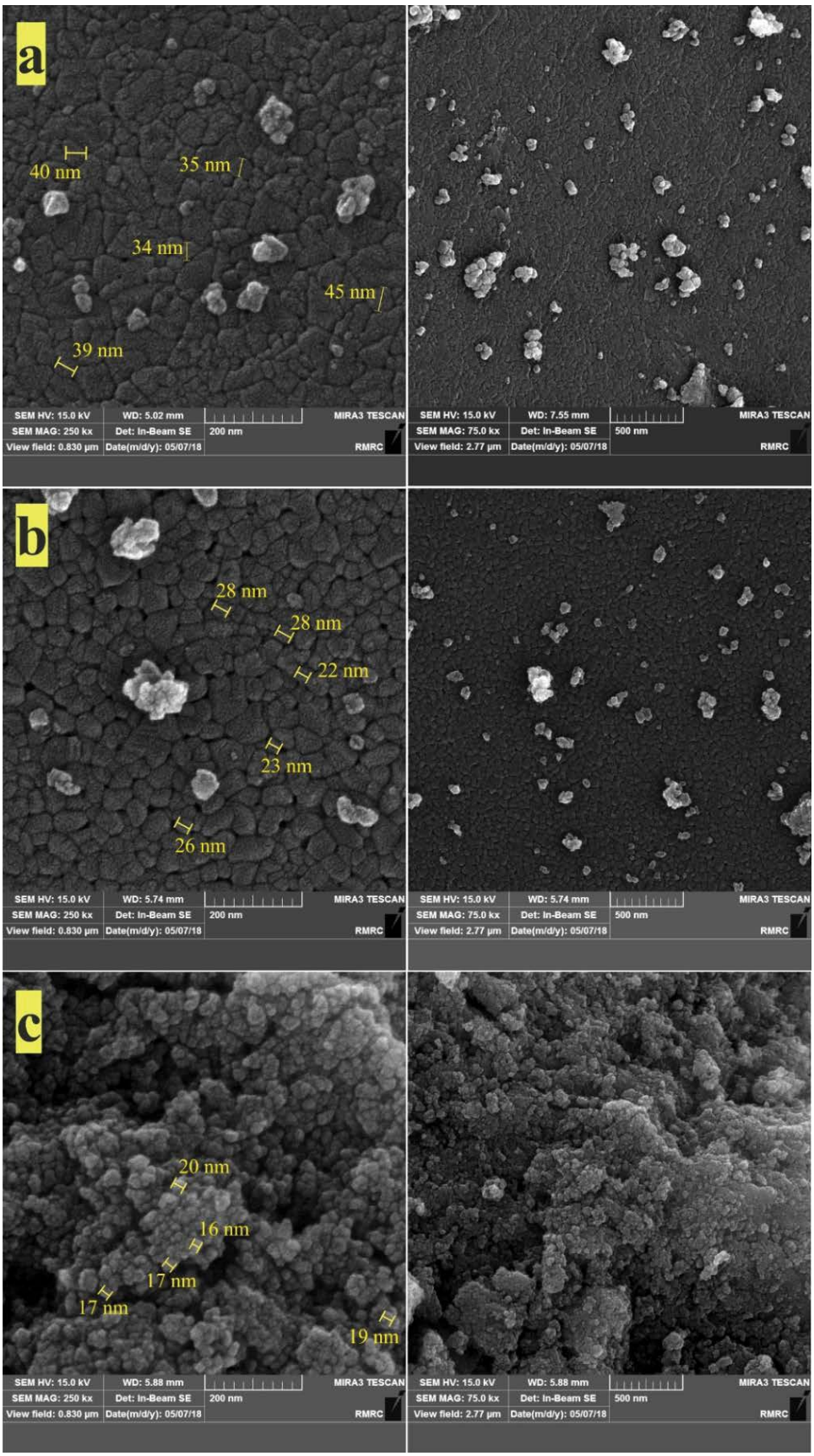

Fig. 5. FE-SEM of samples (a) pure TiO_2, (b) 5.9 (wt.%) Cu-TiO_2, and (c) 5.9 (wt.%) Cu-TiO_2/8.0 (wt.%) Bi_2O_3.

Table 6
Power transform ANOVA results

Source	*F*-value	*P*-value			
Model	761.95	<0.0001	Significant		
A-Bi_2O_3/TiO_2 ratio	4.78	0.0537	Not significant		
B-Cu/Ti ratio	45.64	<0.0001	Significant	R^2	0.998
C-time	3,298.14	<0.0001	Significant	Adj. R^2	0.997
AB	2,820.90	<0.0001	Significant	Pred. R^2	0.993
AC	51.60	<0.0001	Significant	Adeq. precision	107.27
BC	22.57	0.0008	Significant		
A^2	0.71	0.4190	Not significant		
B^2	247.44	<0.0001	Significant		
C^2	10.17	0.0097	Significant		
Lack of fit	0.86	0.5635	Not significant		

Table 7
Power Transform ANOVA results after remove A^2 parameter

Source	*F*-value	*P*-value			
Model	880.27	<0.0001	Significant		
A-Bi_2O_3/TiO_2 ratio	4.91	0.0488	Significant		
B-Cu/Ti ratio	46.88	<0.0001	Significant	R^2	0.998
C-time	3,387.27	<0.0001	Significant	Adj. R^2	0.997
AB	2,897.13	<0.0001	Significant	Pred. R^2	0.994
AC	52.99	<0.0001	Significant	Adeq. precision	114.59
BC	23.18	0.0005	Significant		
B^2	307.72	<0.0001	Significant		
C^2	14.69	0.0028	Significant		
Lack of fit	0.83	0.5943	Not significant		

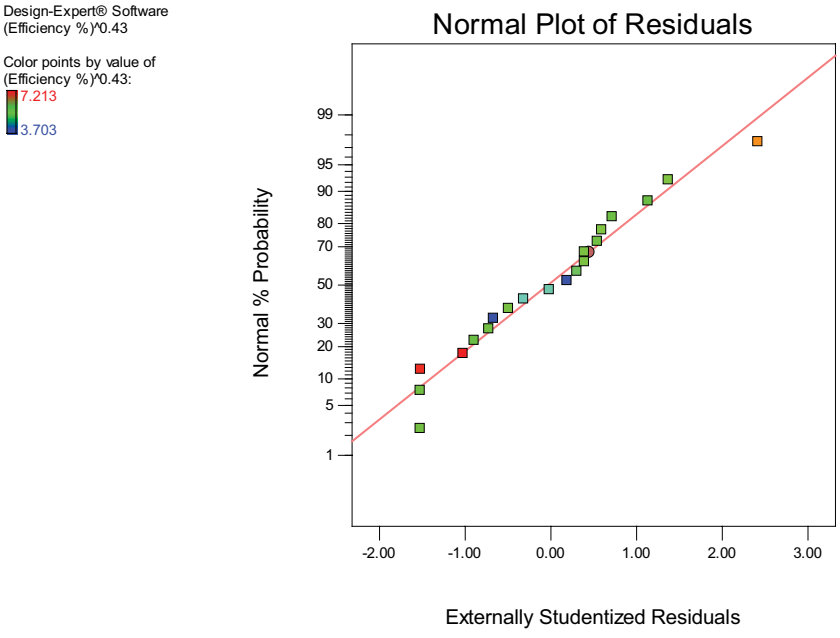

Fig. 6. Normal plot of residual experiments designed by RSM.

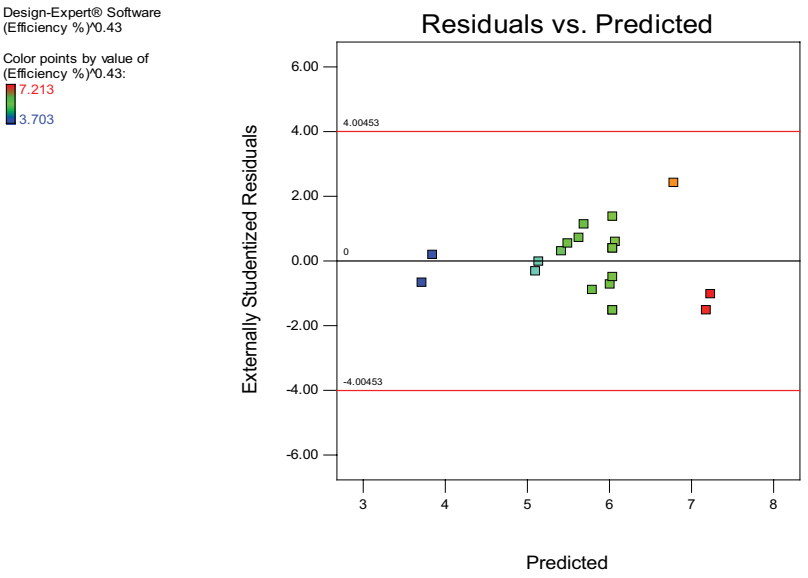

Fig. 7. Plot of the residual vs. model predictions.

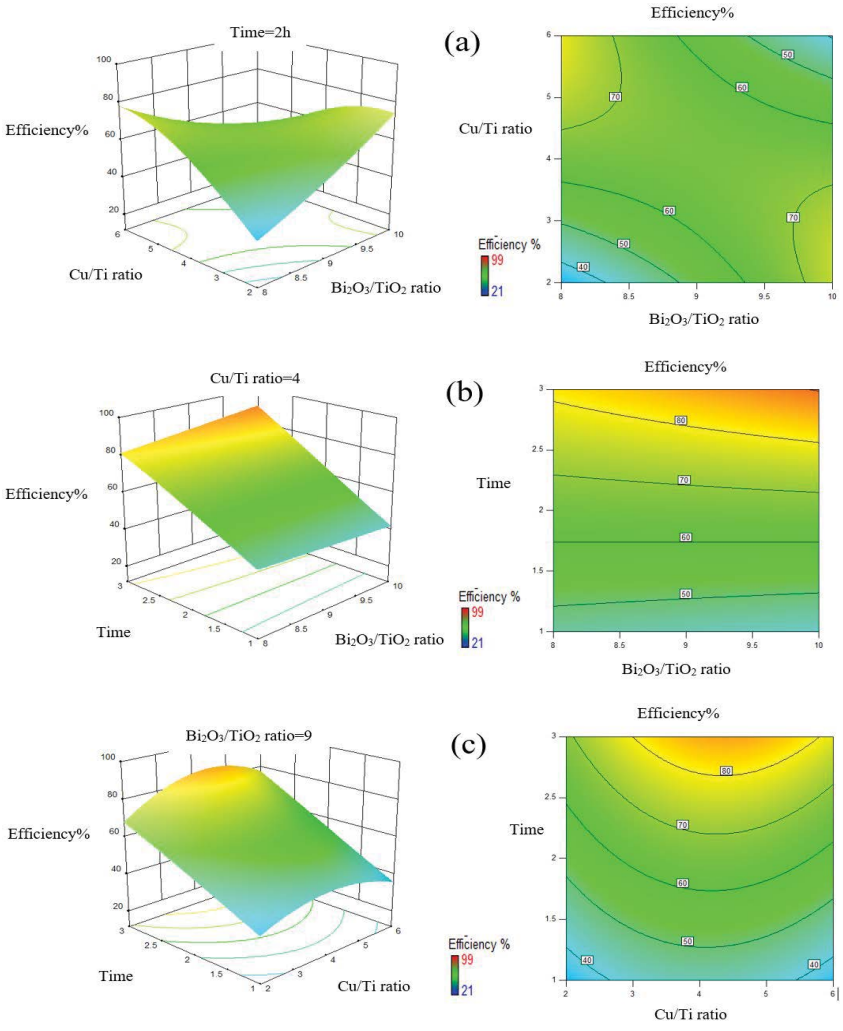

Fig. 8. (a–c) Effects of Cu/Ti, Bi_2O_3/TiO_2 ratios, and reaction time on decolorization efficiency of Direct Red 16.

the reduction of the processing time. Furthermore, at constant the Cu/Ti ratio, by increasing the Bi_2O_3/TiO_2 ratio, the efficiency of decolorization Direct red 16 is enhanced. As shown in Fig. 8c, at a constant Bi_2O_3/TiO_2 ratio, by increasing the Cu/Ti ratio, the decolorization efficiency is initially enhanced and then is reduced. This issue is due to the occurrence of the recombination phenomenon in the nano-catalyst by increasing doping values to an optimum level [35].

3.6. Kinetic study

A kinetic study was done to calculate the constant rate of Direct red 16 photodegradation for pure TiO_2, compared to optimum composites of modified TiO_2 (Cu-TiO_2, Bi_2O_3/TiO_2, and Cu-TiO_2-Bi_2O_3). The pseudo-first-order kinetic model was used to study the photodegradation kinetic for most of the organic molecules as described:

$$-\frac{dc}{dt} = K_{ap}C \tag{5}$$

$$\ln\left(\frac{C_0}{C_t}\right) = K_{ap}t \tag{6}$$

where C_0, C_t, K_{ap}, and t are concentrations at time zero and time t, constant rate, and time, respectively. The kinetic plot ($\ln(C_0/C_t)$ vs. irradiation time) is depicted in Fig. 9. The Cu–TiO_2–Bi_2O_3 indicates a much higher K_{ap} than pure TiO_2, Cu–TiO_2, and Bi_2O_3/TiO_2 which is 31.0, 9.4, and 7.0 times, respectively. It is approved more photocatalytic activity of Cu–TiO_2–Bi_2O_3 nanocomposites.

3.7. Optimization

The suggested model [Eq. (2)] was used to estimate maximum decolorization efficiency, and the corresponding parameters to achieve it. The model predicted a maximum decolorization efficiency of 99.4% under the optimum conditions of the Bi_2O_3/TiO_2 ratio of 8.0 (wt.%), Cu/Ti ratio of 5.9 wt.%, and time of 2.9 h.

In order to confirm the accuracy of the proposed model, four replicate experiments were conducted under the optimum conditions. The decolorization efficiency was found to be 99.0% ± 0.7%, being reasonably close to the predicted value, and the model was successfully validated.

According to the results, the boundary of the lower bounds is considered to be the optimal final, which shows the synergistic effect of the simultaneous presence of Cu and Bi_2O_3 in the nano-catalyst TiO_2. It can be concluded that the shortcoming of TiO_2 nano-catalyst can be resolved by the simultaneous application of Cu and Bi_2O_3.

A comparison is made between the nano-catalyst TiO_2/Bi2O3-Cu and pure TiO_2 efficiencies to investigate the modified nano-catalyst. In two experiments with the same conditions, the efficiency of TiO_2/Bi_2O_3-Cu nano-catalyst is 98%, and pure TiO_2 nano-catalyst efficiency is 38% after 3 h. By comparing these two efficiencies, the effect of the modified nano-catalyst is determined in the process.

3.8. Reusability performance of Cu (5.9 wt.%) doped-TiO_2–Bi_2O_3 (8 wt.%) photocatalyst

Reusability of the Cu (5.9 wt.%) doped-TiO_2–Bi_2O_3 (8 wt.%) photocatalyst for decolorization of Direct red 16 was studied at optimum conditions (initial pH of 6.8, Direct red 16 concentration of 25 mg/L and catalyst loading of 1 g/L) after 3 h. Fig. 10 displays Direct red 16 removal efficiency and recovered photocatalyst (wt.%) for five cycles. After the first cycle, the catalyst was recovered by centrifugation, washed with distilled water, then illuminated under visible light (1 h) to remove the adsorbed pollutants and finally dried at 100°C. The result showed that the photocatalytic activity reduces about 19% after five cycles. It is confirmed that the reused catalyst has a stable structure and could be used in the subsequent runs with relatively sustainable

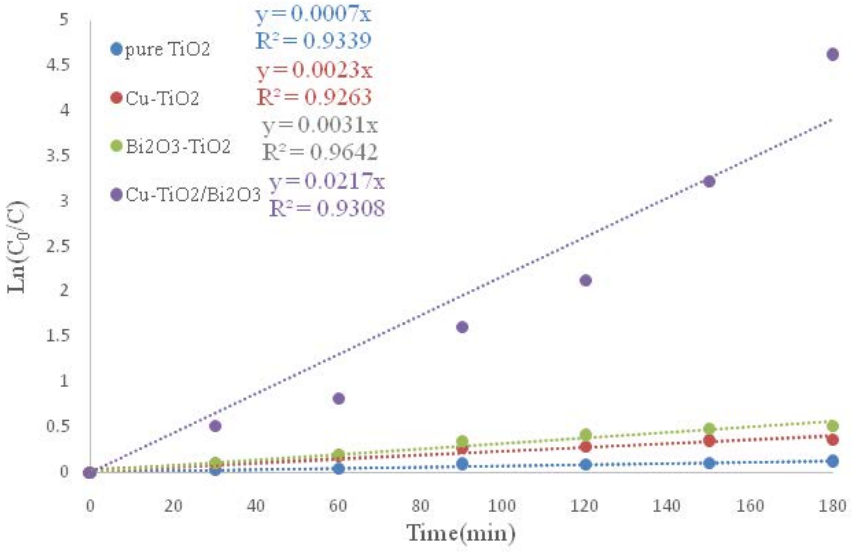

Fig. 9. DR16 photodegradation kinetic (Direct red 16 concentration = 25 mg/L, photocatalyst loading = 1 g/L, and pH of 6.8).

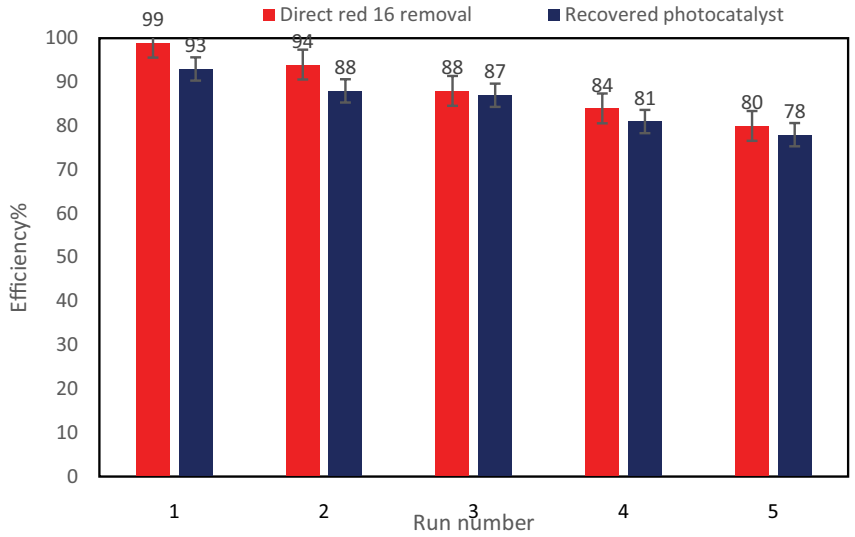

Fig. 10. Reusability results of Cu (5.9 wt.%) doped-TiO_2–Bi_2O_3 (8 wt.%) at pH of 6.8, catalyst loading of 1 g/L, and Direct red 16 concentration of 25 mg/L.

catalytic activity. The recovered photocatalyst was about 80% after five cycles.

4. Conclusions

The sol–gel technology was used in the current study to prepare a set of TiO_2/Bi_2O_3-Cu composites, exhibiting better photocatalytic activities and stability for decolorization of Direct Red 16 dye under visible light radiation. By performing the preliminary tests, the values of Cu/Ti and Bi_2O_3/TiO_2 ratio were determined. The synthesized nano-catalyst with 8 wt.% Bi_2O_3/TiO_2 ratio, 6 wt.% Cu/Ti ratio, and duration of 3 h showed the best performance. Applying a quadratic model derived based by using the RSM method showed that a nano-catalyst with optimum contents of 8.0 wt.% Bi_2O_3/TiO_2 ratio, 5.9 wt.% Cu/Ti ratio and 2.9 h had the best efficiency which is consistent with the results of the performed experiment.

References

[1] K.M. Lee, C.W. Lai, K.S. Ngai, J.C. Juan, Recent developments of zinc oxide based photocatalyst in water treatment technology: a review, Water Res., 88 (2016) 428–448.
[2] O. Chan, W. Cheung, G. McKay, Single and multicomponent acid dye adsorption equilibrium studies on tyre demineralised activated carbon, Chem. Eng. J., 191 (2012) 162–170.
[3] B.R. Shah, U.D. Patel, Aqueous pollutants in water bodies can be photocatalytically reduced by TiO_2 nano-particles in the presence of natural organic matters, Sep. Purif. Technol., 209 (2019) 748–755.
[4] D. Das, D. Charumathi, N. Das, Bioaccumulation of the synthetic dye Basic Violet 3 and heavy metals in single and binary systems by *Candida tropicalis* grown in a sugarcane bagasse extract medium: modelling optimal conditions using response surface methodology (RSM) and inhibition kinetics, J. Hazard. Mater., 186 (2011) 1541–1552.
[5] A. Gupta, A. Pal, C. Sahoo, Photocatalytic degradation of a mixture of Crystal Violet (Basic Violet 3) and Methyl Red dye in aqueous suspensions using Ag+ doped TiO2, Dyes Pigm., 69 (2006) 224–232.
[6] A. Di Paola, E. García-López, G. Marcì, L. Palmisano, A survey of photocatalytic materials for environmental remediation, J. Hazard. Mater., 211 (2012) 3–29.
[7] E. Rafiee, E. Noori, A.A. Zinatizadeh, H. Zangeneh, Surfactant effect on photocatalytic activity of Ag-TiO_2/PW nanocomposite in DR16 degradation: characterization of nanocomposite and RSM process optimization, Mater. Sci. Semicond. Process., 83 (2018) 115–124.
[8] S. Boumaza, F. Kaouah, D. Hamane, M. Trari, S. Omeiri, Z. Bendjama, Visible light assisted decolorization of azo dyes: Direct Red 16 and Direct Blue 71 in aqueous solution on the *p*-$CuFeO_2$/*n*-ZnO system, J. Mol. Catal. A: Chem., 393 (2014) 156–165.
[9] L. Zhang, T. Kanki, N. Sano, A. Toyoda, Photocatalytic degradation of organic compounds in aqueous solution by a TiO_2-coated rotating-drum reactor using solar light, Solar Energy, 70 (2001) 331–337.
[10] M. Tahir, C. Cao, F.K. Butt, F. Idrees, N. Mahmood, Z. Ali, I. Aslam, M. Tanveer, M. Rizwan, T. Mahmood, Tubular graphitic-C_3N_4: a prospective material for energy storage and green photocatalysis, J. Mater. Chem. A, 1 (2013) 13949–13955.
[11] V. Etacheri, C. Di Valentin, J. Schneider, D. Bahnemann, S.C. Pillai, Visible-light activation of TiO_2 photocatalysts: advances in theory and experiments, J. Photochem. Photobiol., C, 25 (2015) 1–29.
[12] T. Hasegawa, P. De Mayo, Surface photochemistry: on the mechanism of the semiconductor-mediated isomerization of 4-substituted cis-stilbenes, Langmuir, 2 (1986) 362–368.
[13] A. Alexiadis, I. Mazzarino, Design guidelines for fixed-bed photocatalytic reactors, Chem. Eng. Process. Process Intensif., 44 (2005) 453–459.
[14] M.M. Zeinabad, S.J. Royaee, M. Sohrabi, Photocatalytic degradation of Reactive Black 8 in UV/TiO_2/H_2O_2 system: optimization and modeling using a response surface methodology (RSM), Afinidad, 70 (2013) 212–219.
[15] A. Fujishima, K. Honda, Electrochemical photolysis of water at a semiconductor electrode, Nature, 238 (1972) 37–38.
[16] A. Fujishima, X. Zhang, D.A. Tryk, TiO_2 photocatalysis and related surface phenomena, Surf. Sci. Rep., 63 (2008) 515–582.
[17] W. Choi, A. Termin, M.R. Hoffmann, The role of metal ion dopants in quantum-sized TiO_2: correlation between photoreactivity and charge carrier recombination dynamics, J. Phys. Chem., 98 (1994) 13669–13679.

[18] A. Hameed, V. Gombac, T. Montini, L. Felisari, P. Fornasiero, Photocatalytic activity of zinc modified Bi_2O_3, Chem. Phys. Lett., 483 (2009) 254–261.
[19] S.G. Kumar, L.G. Devi, Review on modified TiO_2 photocatalysis under UV/visible light: selected results and related mechanisms on interfacial charge carrier transfer dynamics, J. Phys. Chem. A, 115 (2011) 13211–13241.
[20] X. Li, X. Chen, H. Niu, X. Han, T. Zhang, J. Liu, H. Lin, F. Qu, The synthesis of CdS/TiO_2 hetero-nanofibers with enhanced visible photocatalytic activity, J. Colloid Interface Sci., 452 (2015) 89–97.
[21] Y. Liu, F. Xin, F. Wang, S. Luo, X. Yin, Synthesis, characterization, and activities of visible light-driven Bi_2O_3–TiO_2 composite photocatalysts, J. Alloys Compd., 498 (2010) 179–184.
[22] B. Moongraksathum, J.-Y. Shang, Y.-W. Chen, Photocatalytic antibacterial effectiveness of cu-doped TiO_2 thin film prepared via the peroxo sol–gel method, Catalysts, 8 (2018) 352–353.
[23] A. Shojaie, M. Fattahi, S. Jorfi, B. Ghasemi, Hydrothermal synthesis of Fe-TiO_2-Ag nano-sphere for photocatalytic degradation of 4-chlorophenol (4-CP): investigating the effect of hydrothermal temperature and time as well as calcination temperature, J. Environ. Chem. Eng., 5 (2017) 4564–4572.
[24] Y. Cui, X. Zhang, R. Guo, H. Zhang, B. Li, M. Xie, Q. Cheng, X. Cheng, Construction of Bi_2O_3/g-C_3N_4 composite photocatalyst and its enhanced visible light photocatalytic performance and mechanism, Sep. Purif. Technol., 203 (2018) 301–309.
[25] X. Meng, Z. Zhang, Bismuth-based photocatalytic semiconductors: introduction, challenges and possible approaches, J. Mol. Catal. A: Chem., 423 (2016) 533–549.
[26] N.S. Lewis, Toward cost-effective solar energy use, Science, 315 (2007) 798–801.
[27] S. Qiu, S.J. Kalita, Synthesis, processing and characterization of nanocrystalline titanium dioxide, Mater. Sci. Eng., A, 435 (2006) 327–332.
[28] M. Grześkowiak, R. Wróbel, J. Grzechulska, J. Przepiórski, Preparation and characterization of titania powders obtained via hydrolysis of titanium tetraisopropoxide, Mater. Sci. Poland, 32 (2014) 71–79.
[29] J. Spiridonova, A. Katerski, M. Danilson, M. Krichevskaya, M. Krunks, I. Oja Acik, Effect of the titanium isopropoxide: acetylacetone molar ratio on the photocatalytic activity of TiO_2 thin films, Molecules, 24 (2019) 4326–4328.
[30] S. Qourzal, A. Assabbane, Y. Ait-Ichou, Synthesis of TiO_2 via hydrolysis of titanium tetraisopropoxide and its photocatalytic activity on a suspended mixture with activated carbon in the degradation of 2-naphthol, J. Photochem. Photobiol., A, 163 (2004) 317–321.
[31] T. Rojviroon, A. Laobuthee, S. Sirivithayapakorn, Photocatalytic activity of toluene under UV-LED light with TiO_2 thin films, Int. J. Photoenergy, 2012 (2012) 1–8.
[32] M. Ni, M.K. Leung, D.Y. Leung, K. Sumathy, A review and recent developments in photocatalytic water-splitting using TiO_2 for hydrogen production, Renewable Sustainable Energy Rev., 11 (2007) 401–425.
[33] M.I. Litter, Heterogeneous photocatalysis: transition metal ions in photocatalytic systems, Appl. Catal., B, 23 (1999) 89–114.
[34] V. Koteski, J. Belošević-Čavor, A. Umićević, V. Ivanovski, D. Toprek, Improving the photocatalytic properties of anatase TiO_2 (101) surface by co-doping with Cu and N:Ab initio study, Appl. Surf. Sci., 425 (2017) 1095–1100.
[35] S. Jorfi, S. Mirali, A. Mostoufi, M. Ahmadi, Visible light photocatalytic degradation of azo dye and a real textile wastewater using Mn, Mo, La/TiO_2/AC nanocomposite, Chem. Biochem. Eng. Q., 32 (2018) 215–227.